Indonesian Journal of Science & Technology

Journal homepage: http://ejournal.upi.edu/index.php/ijost/

# Optimization by Artificial Neural Network (ANN) of Malachite Green Adsorption on Clays: Contribution to the Achievement of the Sustainable Development Goals (SDGs)

*Aouda Bounif[1], Houria Rezala[1,*], Omar Bouras[2]*

[1]Djilali Bounaama University of Khemis Miliana, Khemis-Miliana, Algeria
[2]Universite Blida 1, Blida, Algeria
*Correspondence: E-mail: rezala_houria@hotmail.com

## ABSTRACT

This study focused on the adsorption of malachite green onto clays in aqueous solutions. The results were simulated using an artificial neural network (ANN). Materials were characterized using X-ray fluorescence spectrometry, Fourier transform infrared spectroscopy, X-ray diffraction, and nitrogen adsorption at 77 K. Sorption experiments were carried out in the discontinuous mode, examining the influences of contact time, adsorbent dose, solution pH, initial concentration, and temperature. The neural network topology was 4–10-1. The results predicted by this model show a good agreement with experimental data. The mathematical modelling of the obtained isotherms revealed that the Freundlich isotherm model is perfectly consistent with the experimental data. The thermodynamic parameters, such as the changes in Gibbs free energy, enthalpy, and entropy, are determined. The MG adsorption is physical, spontaneous, and exothermic for both adsorbents. This method, therefore, appears as an effective means to achieve the objectives of sustainable development of the United Nations.



## ARTICLE INFO

***Article History:***
*Submitted/Received 15 Jan 2026*
*First Revised 20 Feb 2026*
*Accepted 09 Mar 2026*
*First Available Online 10 Mar 2026*
*Publication Date 01 Apr 2026*

***Keyword:***
*Adsorption,*
*Artificial intelligence,*
*Bentonite,*
*Malachite green,*
*Optimization.*

## 1. INTRODUCTION

Organic dyes play an important role in various applications and are therefore responsible for toxic pollution of the environment. These releases of synthetic organic dyes pose a great problem for the environment and human health as they are not biodegradable for the most part [1-3]. Among the different types of dyes, Malachite Green (MG) is used in the textile industry to color leather, silk, wool, jute, pottery, cotton, acrylic fibers, and paper. It is a carcinogenic, mutagenic, and teratogenic substance, and it has been identified as a liver tumor promoter [4]. MG is light stable and poorly biodegradable, making it difficult to remove from aqueous solutions by current water purification/treatment methods. Among all the used methods, adsorption has become the most desirable technique because of its advantages in terms of low cost, ease of use, simplicity of design, and insensitivity to toxic pollutants [5]. In this context, many adsorbents have been used to remove these dyes from water, including activated carbon [6], zeolite [7,8], graphene [9], silica [10], metal-organic frameworks [11], and clays [12]. In addition, numerous studies have extensively explored the use of crude and or modified clays for the adsorption of organic dyes due to their cost-effectiveness, abundance in nature, and high efficiency. Among all these clays, bentonite has gained significant recognition as an effective adsorbent. Despite the good performance of bentonite in the adsorption of organic dyes, experimental data remain, however, long and costly. Artificial neural network (ANN) is a powerful artificial intelligence approach in modeling and predicting data and has been gaining interest in the investigation of adsorption processes [13]. In this context, the ANN with 10 hidden 10-hidden-layer neuron combination to predict the adsorption performance of almond peel waste as a sorbent against malachite green and were able to obtain a remarkable coefficient of determination ($R^2$) value of 0.976 [14]. Wang *et al*. (2024) [15] employed the ANN to predict the adsorption performance of ZIF-67 on malachite green, with a remarkable $R^2$ of 0.9882 and mean square error (MSE) of 0.0009. Parsazadeh *et al*. (2018) [16] used the ANN with 6 hidden layer neurons to predict the adsorption efficiency of both eosin yellow (EY) and malachite green (MG) dyes in binary aqueous solution onto the monolithic HKUST-1 MOF. Corresponding $R^2$ values of 0.9974 and 0.9963 and MSE values of $1.75\times10^{-5}$ and $7.43\times10^{-5}$ were obtained for the MG and EY models, respectively. To date, there is no report on the use of ANN to predict malachite green adsorption performance on clays.

In this context, this present work aims to investigate the adsorption of MG from aqueous solutions onto both local Algerian bentonite and another commercial clay. The effects of different parameters that can influence the elimination percentage of MG, in aqueous solutions, were studied through several adsorption tests in discontinuous systems. Indeed, these parameters can be expressed as a major problem where there could be a complex relationship between the inputs (contact time, solution pH, adsorbent dose, MG initial concentration, and temperature) and outputs (removal percentage). Under such conditions, the application of ANN appears to be the most useful method in the interpretation of optimum parameters favoring the best sorption of MG molecules on the used sorbent clays.

ANN appears effective since it offers predictive data, estimates, and opportunities in the treatment of dye rejections with high precision. Its techno-economic value as well as its cost estimate allow it to contribute to the sustainable development goals, in particular goal 6 on access to water and sanitation. Thus, it contributes to the improvement of water quality by reducing its pollution and minimizing the release of dangerous chemicals.

DOI: https://doi.org/10.17509/ijost.v11i1.87371
p- ISSN 2528-1410 e- ISSN 2527-8045

## 2. METHODS

### 2.1. Material and Chemicals

The raw bentonite used in this study was extracted from Maghnia deposits in western Algeria. Initially, it was purified according to the method previously reported [17]. The adsorptive properties of the resulting fraction < 2 µm, which is designated "local Algerian bentonite'' were compared to those of a commercial bentonite.

The MG dye (chemical formula $C_{23}H_{25}ClN_2$, molecular weight = 364.911 g/mol, λmax = 617 nm, solubility in water = 40 g/L, pKa1 = 1.3 and pKa2 ≈ 12.5), as well as chemicals (NaOH, $H_2SO_4$) and commercial bentonite with the highest purity available were obtained from Biochem Chemopharma company, France and used as received. All the solutions were prepared using distilled water. The chemical structure of the MG is shown in **Figure 1**.

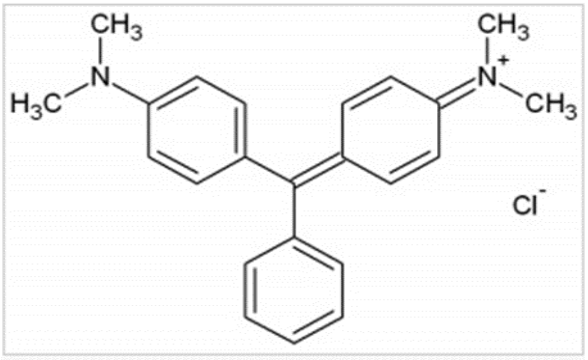


**Figure 1.** Molecular structure of MG.

### 2.2. Characterization Methods

Chemical composition of the samples was determined by X-ray fluorescence spectrometry (PHILIPS-PW2404 Pananalytical, Magix-Pro model) of 4 KW of power equipped with logging data software. Semiquantitative measurements were made with the Ommian application using 27 mm sample holders with a full range measurement sweep. The Fourier transform infrared (FTIR) spectra of the samples were obtained using a SPECTRUM TWO spectrometer (Perkin Elmer, Inc.). ZnSe (550–6000 $cm^{-1}$) and KBr (350–8300 $cm^{-1}$) pellets were used in transmission mode for this. The XRD study was obtained using a diffractometer (PHILIPS, PW-1711) equipped with CuKα radiation (l = 0.15404 nm). Using nitrogen as the sorbate gas at 77 K, the textural qualities were measured using a Quantachrome Quadrasorb SI system. The samples were outgassed for 18 hours at 373 K under a high vacuum ($10^{-2}$ Torr). Total specific surface areas were calculated using the multipoint BET method.

### 2.3. Adsorption Experiments

The various adsorption tests were carried out in discontinuous mode. The effect of contact time, ranging from 1 to 60 min, was examined in several mixtures of 25 mg of commercial bentonite or local Algerian bentonite in 25 mL of MG solution with an initial concentration of 100 mg/L in flasks. The whole is subjected to the same agitation of 150 rpm in a shaker (Memmert). These mixtures were then centrifuged at 2000 rpm for 15 minutes to separate the two phases and recover the solid phases corresponding to the saturated adsorbents. All obtained supernatants were analyzed by UV–Vis spectrophotometer (Genesys-10 UV) at the maximum absorption wavelength of MG (λmax = 617 nm).

The MG concentrations of different samples were determined by extrapolation on the calibration curve obtained previously by plotting the absorbance values as a function of the

DOI: https://doi.org/10.17509/ijost.v11i1.87371
p- ISSN 2528-1410 e- ISSN 2527-8045

MG concentration. The removal percentages of the MG were calculated according to the following Eq. (1):

$$Removal\ percentage = \frac{(C_o - C_e)}{C_o} \times 100 \quad (1)$$

Where, $C_o$ and $C_e$ (mg/L) are the concentrations of MG at the initial and equilibrium states, respectively.

The effect of adsorbent dose was investigated using various amounts (ranging from 5 to 50 mg) of commercial bentonite or local Algerian bentonite that has been dispersed into 25 mL of MG solution with an initial concentration of 100 mg/L. Each dispersion was shaken for 5 min at ambient temperature (25 ± 1°C). The effect of pH on the adsorption was examined by adjusting the pH of different suspensions between 2 and 10. A series of mixtures (30 mg of local Algerian bentonite or 15 mg of commercial bentonite) and 25 mL of MG solutions with an initial concentration of 100 mg/L) were stirred at 150 rpm for 5 min. The pH of MG solutions was adjusted using a few drops of $H_2SO_4$ (0.1 mol/L) or a few drops of NaOH (0.1 mol/L) aqueous solutions, and the corresponding values were measured using a pH meter (Basic 20). The effect of MG initial concentration was carried out by mixing a series of 30 mg of local Algerian bentonite or 15 mg of commercial bentonite in a series of 25 mL of MG solutions at different concentrations (from 4 to 200 mg/L) during the contact time under agitation for 5 min at the natural pH of the solutions (pH = 7). The effect of temperature was examined by MG adsorption at different temperatures (20, 30, 40, and 50°C) at natural pH (pH = 7) of the solutions, 30 mg of local Algerian bentonite or 15 mg of commercial bentonite as adsorbent mass, and 5 min as contact time.

### 2.4. Artificial Neural Network (ANN)

The ANN model was used to simulate the adsorption process of commercial bentonite and local Algerian bentonite on malachite green dye. The ANN structure principally consists of layers that comprise input, hidden, and output layers. Each of these layers is composed of units called neurons. The input layer receives data from the outside source that the neural network needs to analyze or learn about. The data goes through hidden layers that transform the input into data that is helpful for the output layer, and the last layer produces the final prediction or result. The feedforward neural network was created to adjust the weights of the neurons to minimize the error between the predicted and the real output. This process was carried out employing backpropagation and gradient descent.

In this study, the neural device used is 4, 10, and 1, which are assigned to the number of neurons in the input, output, and masking layers, respectively. For both clays (commercial and Algerian bentonite), the input data are 22 and 20 values for training, 5 and 4 values for validation, and 5 and 4 values for test, which make up 70, 15, and 15% of the total data, respectively. **Figure 2** shows the illustration of the ANN structure.

The neural network tool in MATLAB was used to evaluate the ANN (feedforwardnet). The data were normalized using Eq. (2) [15].

$$X_i^* = \frac{X_i - X_{min}}{X_{max} - X_{min}} \quad (2)$$

Where, $X_i^*$ is the normalized adsorption variable, $X_{max}$ and $X_{min}$ are the maximum and minimum values of $X_i$, respectively.

**Tables 1** and **2** illustrate the input dataset for the neural network, which contains feed initial MG concentration, solution pH, adsorbent dose, and contact time as input parameters. In the context of the optimization of malachite green adsorption from aqueous solutions, the use of ANN is essential since the problem cannot be modeled by simple linear relations or defined by explicit rules. ANNs appear to be excellent not only in complex non-linear

DOI: https://doi.org/10.17509/ijost.v11i1.87371
p- ISSN 2528-1410 e- ISSN 2527-8045

relationships directly from the data, but also to eliminate the need to program all possible scenarios. Their ability to continuously adapt and improve their performance with new data, even in variable environments, and to generalize effectively to new situations, makes them particularly relevant. Moreover, unlike traditional algorithms that struggle with imperfect data, ANNs efficiently handle noisy or incomplete information while providing reliable predictions or classifications despite inaccuracies. This ability for learning by example and generalizing, combined with their central role in artificial intelligence for high-precision optimizations, predictions, and classifications, fully justifies their use to model our application, reflecting many research disciplines that are turning to artificial intelligence.

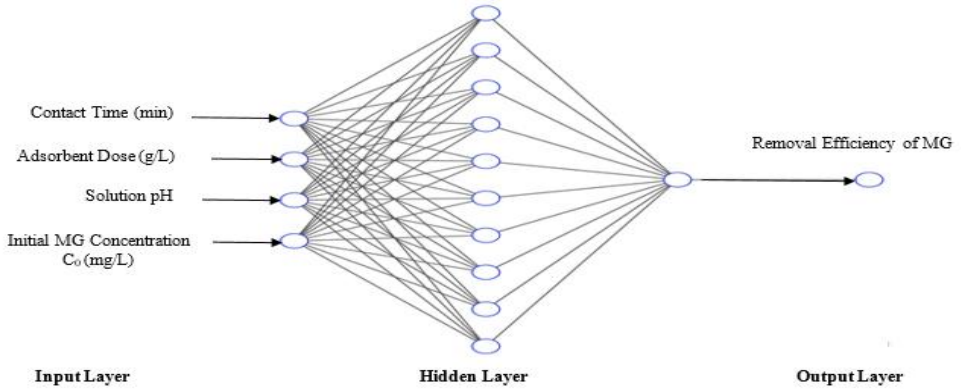


**Figure 2.** Schematic illustration of ANN structure (input, hidden, and output layers).

**Table 1.** Experimental conditions of commercial bentonite for AI-based modeling.

| $N_0$ | MG initial concentration $C_0$ (mg/L) | Solution pH | Adsorbent dose (g/L) | Contact time (min) |
|---|---|---|---|---|
| 1 | 100 | 3.9 | 1 | 1 |
| 2 | 100 | 3.9 | 1 | 2 |
| 3 | 100 | 3.9 | 1 | 3 |
| 4 | 100 | 3.9 | 1 | 4 |
| 5 | 100 | 3.9 | 1 | 5 |
| 6 | 100 | 3.9 | 1 | 10 |
| 7 | 100 | 3.9 | 1 | 15 |
| 8 | 100 | 3.9 | 1 | 20 |
| 9 | 100 | 3.9 | 1 | 30 |
| 10 | 100 | 3.9 | 1 | 60 |
| 11 | 100 | 3.9 | 0.2 | 5 |
| 12 | 100 | 3.9 | 0.4 | 5 |
| 13 | 100 | 3.9 | 0.6 | 5 |
| 14 | 100 | 3.9 | 0.8 | 5 |
| 15 | 100 | 3.9 | 1 | 5 |
| 16 | 100 | 3.9 | 1.2 | 5 |
| 17 | 100 | 3.9 | 1.6 | 5 |
| 18 | 100 | 3.9 | 2 | 5 |
| 19 | 100 | 2 | 0.6 | 5 |
| 20 | 100 | 4 | 0.6 | 5 |
| 21 | 100 | 6 | 0.6 | 5 |
| 22 | 100 | 7 | 0.6 | 5 |
| 23 | 100 | 8 | 0.6 | 5 |
| 24 | 100 | 10 | 0.6 | 5 |

DOI: https://doi.org/10.17509/ijost.v11i1.87371
p- ISSN 2528-1410 e- ISSN 2527-8045

**Table 1 (continue).** Experimental conditions of commercial bentonite for AI-based modeling.

| $N_0$ | MG initial concentration $C_0$ (mg/L) | Solution pH | Adsorbent dose (g/L) | Contact time (min) |
|---|---|---|---|---|
| 25 | 4 | 3.9 | 0.6 | 5 |
| 26 | 10 | 3.9 | 0.6 | 5 |
| 27 | 20 | 3.9 | 0.6 | 5 |
| 28 | 40 | 3.9 | 0.6 | 5 |
| 29 | 80 | 3.9 | 0.6 | 5 |
| 30 | 100 | 3.9 | 0.6 | 5 |
| 31 | 200 | 3.9 | 0.6 | 5 |
| 32 | 300 | 3.9 | 0.6 | 5 |

**Table 2.** Experimental conditions of local Algerian bentonite for AI-based modelling.

| $N_0$ | MG initial concentration $C_0$ (mg/L) | Solution pH | Adsorbent dose (g/L) | Contact time (min) |
|---|---|---|---|---|
| 1 | 100 | 3.9 | 1 | 5 |
| 2 | 100 | 3.9 | 1 | 10 |
| 3 | 100 | 3.9 | 1 | 15 |
| 4 | 100 | 3.9 | 1 | 25 |
| 5 | 100 | 3.9 | 1 | 30 |
| 6 | 100 | 3.9 | 1 | 60 |
| 7 | 100 | 3.9 | 0.2 | 5 |
| 8 | 100 | 3.9 | 0.4 | 5 |
| 9 | 100 | 3.9 | 0.6 | 5 |
| 10 | 100 | 3.9 | 0.8 | 5 |
| 11 | 100 | 3.9 | 1 | 5 |
| 12 | 100 | 3.9 | 1.2 | 5 |
| 13 | 100 | 3.9 | 1.6 | 5 |
| 14 | 100 | 3.9 | 2 | 5 |
| 15 | 100 | 2 | 1.2 | 5 |
| 16 | 100 | 4 | 1.2 | 5 |
| 17 | 100 | 6 | 1.2 | 5 |
| 18 | 100 | 7 | 1.2 | 5 |
| 19 | 100 | 8 | 1.2 | 5 |
| 20 | 100 | 10 | 1.2 | 5 |
| 21 | 4 | 3.9 | 1.2 | 5 |
| 22 | 10 | 3.9 | 1.2 | 5 |
| 23 | 20 | 3.9 | 1.2 | 5 |
| 24 | 40 | 3.9 | 1.2 | 5 |
| 25 | 80 | 3.9 | 1.2 | 5 |
| 26 | 100 | 3.9 | 1.2 | 5 |
| 27 | 200 | 3.9 | 1.2 | 5 |
| 28 | 300 | 3.9 | 1.2 | 5 |

## 3. RESULTS AND DISCUSSION

### 3.1. Characterization of The Materials

The X-ray fluorescence data for both used clays (Algerian bentonite and commercial bentonite) are presented in **Table 3**. Comparatively, the value of the $SiO_2/Al_2O_3$ ratio (maximum substitution of $Si^{4+}$ by $Al^{3+}$) is about 3.3 for Algerian bentonite which remains higher than that of conventional bentonites (r = 2.7) and thus confirms previous results that highlight the co-existence of free quartz in the clay fraction [18].

DOI: https://doi.org/10.17509/ijost.v11i1.87371
p- ISSN 2528-1410 e- ISSN 2527-8045

X-ray diffraction patterns as well as the basal spacings of the two used bentonites are illustrated in **Figure 3(a)** and **Table 3**. As these diffractograms show, the peak corresponding to the reflection (001) of montmorillonite appears at 2θ angles (2θ ≈ 7). This result indicates that the main interlayer cation in both bentonites is sodium (12.5 Å of local Algerian bentonite and 12.55 Å of the commercial bentonite, see **Table 1**), which is consistent with the XRF analysis results. Similar findings have been previously reported [19,20].

The textural properties of the two used clays are shown in **Table 3**. The commercial bentonite displays a BET specific surface area and pore volume, substantially higher than that of local Algerian bentonite. Additionally, it was observed that the commercial bentonite present high values of micropore surface area and micropore volume, in line with previous studies, demonstrating that the micropore are known to contribute to most of the adsorption capacity [21].

**Table 3.** Chemical composition (wt%), basal spacing (d001), and textural properties of the two used clays [5,22,23].

| Adsorbent | Chemical Composition (Wt%) | | | | Textural Properties | | | |
|---|---|---|---|---|---|---|---|---|
| | $Al_2O_3$ | $SiO_2$ | $Na_2O$ | $d_{001}$ (Å) | BET specific surface area ($m^2/g$) | Micropore Surface Area ($m^2/g$) | Micropore volume ($cm^3/g$) | Pore volume ($cm^3/g$) |
| **Local Algerian bentonite** | 17.75 | 58.52 | 2.72 | 12.5 | 59.3 | 13.0 | 0.009 | 0.11 |
| **Commercial bentonite** | 17.86 | 47.70 | 2.43 | 12.55 | 76.97 | 27 | 0.013 | 1.15 |

**Figure 3b** shows the nitrogen adsorption–desorption isotherm of commercial bentonite and local Algerian bentonite. When the relative pressures were low (P/P0 < 0.5), the isotherm exhibited type I isotherms as classified by Brunauer, Deming, Deming, and Teller (BDDT) [24], which is characteristic of microporous systems [25]. Nevertheless, the isotherm is correlated with the type IV class when the P/P0 value is greater, indicating that the system has a wide range of pore sizes. The identification of hysteresis loops, type H3 as described by Sing et al. (1985) [25], suggests the existence of mesoporosity inside these materials.

The FTIR spectra of the used clays appearing in the range of 4000–400 $cm^{-1}$ are shown in **Figure 3c**. The band appearing at 3690 $cm^{-1}$ is attributed to the vibrations of the Si-OH bond. The band at about 3625 $cm^{-1}$ corresponds to the stretching vibration of octahedral O-H groups, attached to $Al^{3+}$ or $Mg^{2+}$ [26]. The band at 1634 $cm^{-1}$ corresponds to H–O–H deformation vibrations of water. The most intense band at 997 $cm^{-1}$ is attributed to the asymmetric Si–O–Si stretching vibrations of the tetrahedral sheet. The occupancy of the octahedral sheets is indicated by the 913 $cm^{-1}$ band, representing Al–Al–OH bending vibrations. The montmorillonite is characterized by the bands at 516 and 461 $cm^{-1}$, which correspond to the bending and stretching vibrations of Si-O bonds, respectively.

DOI: https://doi.org/10.17509/ijost.v11i1.87371
p- ISSN 2528-1410 e- ISSN 2527-8045

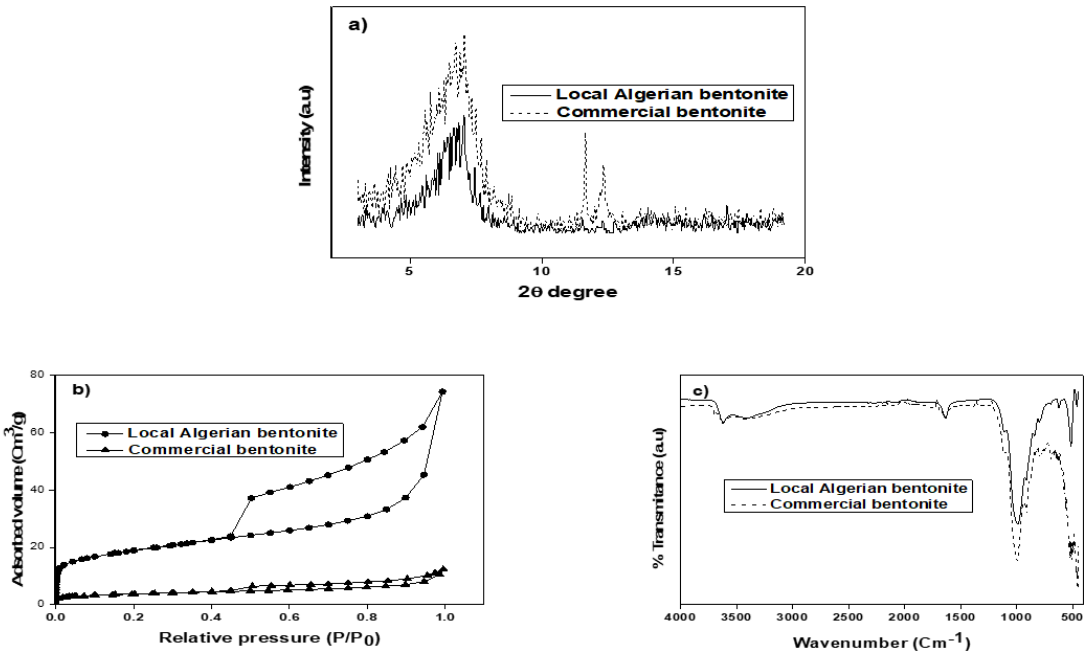


**Figure 3.** a) XRD patterns of used clays; b) N2 adsorption–desorption isotherms of used clays; c) FTIR spectra of used clays.

### 3.2. ANN Optimization

The results of the normalized data of the fitnet neural network optimization are shown in **Figure 4**.

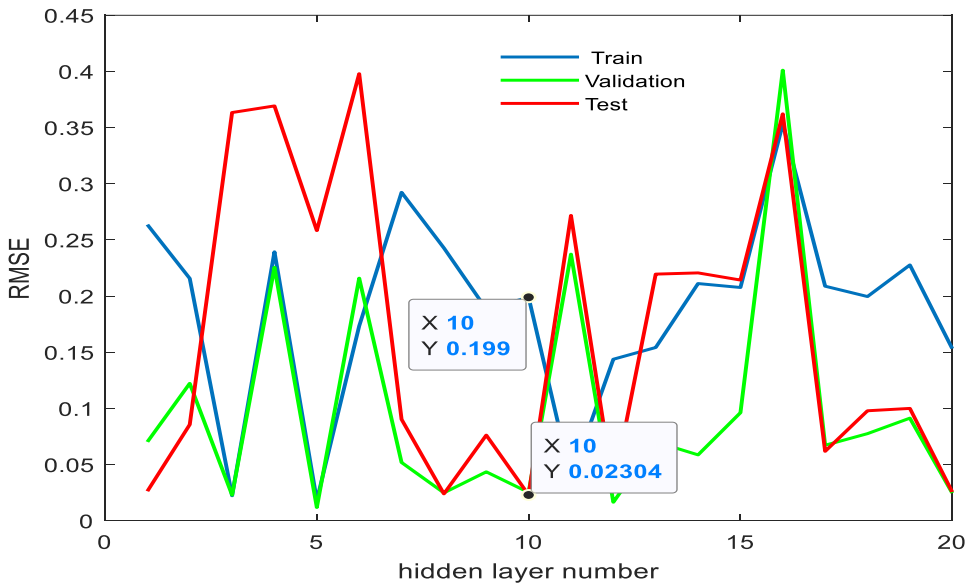


**Figure 4.** Normalized data of the fitnet neural network optimization.

This figure shows that the optimal number of neurons (giving minimum prediction error) in the hidden layer is 10. The best neural network topology was 4-10-1, four input neurons (four parameters including contact time, adsorbent dose, solution pH, and initial malachite green concentration); ten neurons hidden in a layer, and one output neuron (designating removal MG percentage). The prediction error for the learning phase in blue color equals 0.199. The prediction error for the validation and test phases in green and red colors is equal

DOI: https://doi.org/10.17509/ijost.v11i1.87371
p- ISSN 2528-1410 e- ISSN 2527-8045

to 0.023. The results of the normalized data of feedforward neural network optimization are shown in **Figure 5**.

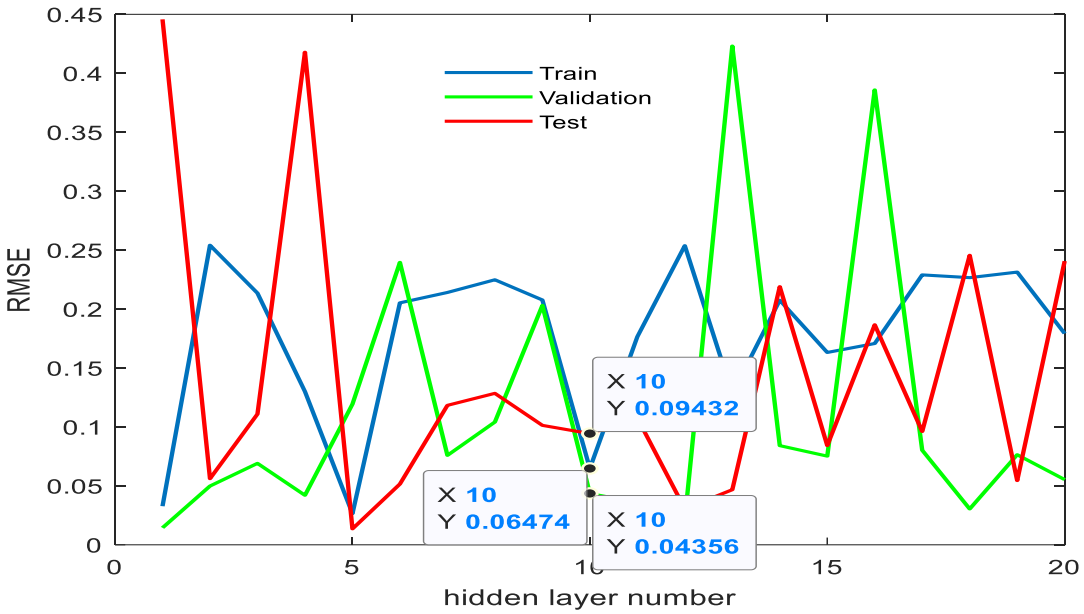


**Figure 5.** Normalized data of feedforward neural network optimization.

These figures are optional, just to justify the choice of network architecture. **Figure 2** above is the best case for a single hidden layer; therefore, we worked with it.

To evaluate the model's performance, we applied the correlation coefficient (R) and mean square error (MSE). R is used to assess the strength of associations between data variables. MSE is used to measure model prediction errors and to assess the difference between the predicted and actual values. The predictive modeling outcomes of neural network computations are presented in **Tables 4** and **5**.

**Table 4.** Evaluation of predictive modeling outcomes of commercial bentonite.

| Number of neurons | ANN at different stages | Sample | MSE | R | Overall performance | Overall R |
|---|---|---|---|---|---|---|
| 5 | Train | 22 | 0.0525 | 0.6864 | | |
| | Validation | 5 | 0.0165 | 0.6370 | 0.0409 | 0.6519 |
| | Testing | 5 | 0.0142 | 0.8030 | | |
| 6 | Train | 22 | $2.0819\times10^{-4}$ | 0.9938 | | |
| | Validation | 5 | 0.1236 | 0.9544 | 0.0211 | 0.6938 |
| | Testing | 5 | 0.0106 | 0.9126 | | |
| 7 | Train | 22 | $7.6509\times10^{-4}$ | 0.9774 | | |
| | Validation | 5 | 0.0016 | 0.5057 | 0.0207 | 0.6977 |
| | Testing | 5 | 0.1276 | 0.9188 | | |
| 8 | Train | 22 | 0.0264 | 0.7053 | | |
| | Validation | 5 | 0.0024 | 0.8778 | 0.0189 | 0.7120 |
| | Testing | 5 | 0.0021 | 0.6833 | | |
| 9 | Train | 22 | 0.0268 | 0.6240 | | |
| | Validation | 5 | 0.0274 | 0.8087 | 0.0230 | 0.6367 |
| | Testing | 5 | 0.0016 | -0.0195 | | |
| 10 | Train | 22 | 0.0025 | 0.9158 | | |
| | Validation | 5 | 0.1541 | 0.8231 | 0.0263 | 0.6110 |
| | Testing | 5 | 0.0034 | 0.8961 | | |

DOI: https://doi.org/10.17509/ijost.v11i1.87371
p- ISSN 2528-1410 e- ISSN 2527-8045

**Table 5.** Evaluation of predictive modeling outcomes of local Algerian bentonite.

| Number of neurons | ANN at different stages | Sample | MSE | R | Overall performance | Overall R |
|---|---|---|---|---|---|---|
| 5 | Train | 20 | $3.2267\times10^{-4}$ | 0.9985 | | |
| | Validation | 4 | 0.0037 | 0.9540 | 0.0027 | 0.9873 |
| | Testing | 4 | 0.0136 | 0.8265 | | |
| 6 | Train | 20 | $7.1256\times10^{-5}$ | 0.9995 | | |
| | Validation | 4 | $5.5563\times10^{-4}$ | 0.9988 | 0.0025 | 0.9900 |
| | Testing | 4 | 0.0164 | 0.9922 | | |
| 7 | Train | 20 | $4.6797\times10^{-5}$ | 0.9998 | | |
| | Validation | 4 | $3.7500\times10^{-4}$ | 0.9977 | 0.0016 | 0.9920 |
| | Testing | 4 | 0.0106 | 0.9696 | | |
| 8 | Train | 20 | $2.1517\times10^{-4}$ | 0.9992 | | |
| | Validation | 4 | $8.5405\times10^{-4}$ | 0.9897 | 0.0065 | 0.9716 |
| | Testing | 4 | 0.0438 | 0.8704 | | |
| 9 | Train | 22 | 0.0010 | 0.9946 | 0.0010 | 0.9948 |
| | Validation | 5 | $5.9489\times10^{-4}$ | 0.9994 | | |
| | Testing | 5 | 0.0016 | 0.9858 | | |
| 10 | Train | 20 | $2.6489\times10^{-4}$ | 0.9988 | | |
| | Validation | 4 | 0.0128 | 0.8266 | 0.0051 | 0.9742 |
| | Testing | 4 | 0.0218 | 0.6596 | | |

The observed low MSE values and acceptable R values indicated good performance, given by the ANN structure with 10 neurons in the hidden layer for commercial bentonite and 7 neurons in the hidden layer for local Algerian bentonite. Based on data for commercial bentonite (MSE = 0.0025; R = 0.9158) and local Algerian bentonite (MSE = $4.6797\times10^{-5}$; R = 0.9998), the network training is considered good. On the other hand, we noticed that there is a slowly decrease in performance for the validation (MSE = 0.1541, R = 0.8231 for commercial bentonite and MSE = $3.7500\times10^{-4}$, R = 0.9977 for local Algerian bentonite) and the testing (MSE = 0.0034, R = 0.8961 for commercial bentonite and MSE = 0.0106, R = 0.9696 for local Algerian bentonite) compared to the training because the validation and testing data are new to the network. Overall, these tables reveal that the ANN model can correlate well with the experimental values of the MG adsorption onto the two adsorbents.

### 3.3. MG Adsorption on Used Clays

The effect of different parameters on the MG adsorption was studied by parametric analysis. F**igures 6** to **10** present the experimental results and their comparison with ANN ANN-predicted values.

#### 3.3.1. Effect of contact time

Contact time is an important parameter as it can determine the time required to reach thermodynamic equilibrium for the adsorption process and predict the feasibility of an adsorbent for use in wastewater treatment. The removal efficiencies of MG on samples from aqueous solution as a function of contact time are depicted in **Figure 6**. As observed, the results revealed that removal efficiency rapidly increased within the first 1 min for commercial bentonite and 5 min for local Algerian bentonite and reached adsorption equilibrium thereafter. This can be interpreted by the fact that, at the start of adsorption, the number of active sites available on the surface of the adsorbent material is much greater than that remaining after a certain time. The final adsorption capacities were calculated to be approximately 99 % and 86% for commercial bentonite and local Algerian bentonite,

DOI: https://doi.org/10.17509/ijost.v11i1.87371
p- ISSN 2528-1410 e- ISSN 2527-8045

respectively. Subsequently, no further adsorption was observed. Therefore, a contact time of 5 min for the two adsorbents was deemed sufficient for subsequent experiments. Compared with the literature, this equilibrium time is better than the ones previously reported [15]. However, the commercial bentonite has a higher adsorption capacity than the local Algerian bentonite. It can be related to the high values of micropore surface area and micropore volume for commercial bentonite, and consequently, increased adsorption capacity. The predicted data were in good agreement with the experimental values.

The adsorption kinetics of MG by the two used clays were not achieved due to the very fast rate, and reached equilibrium within the first 5 minutes.

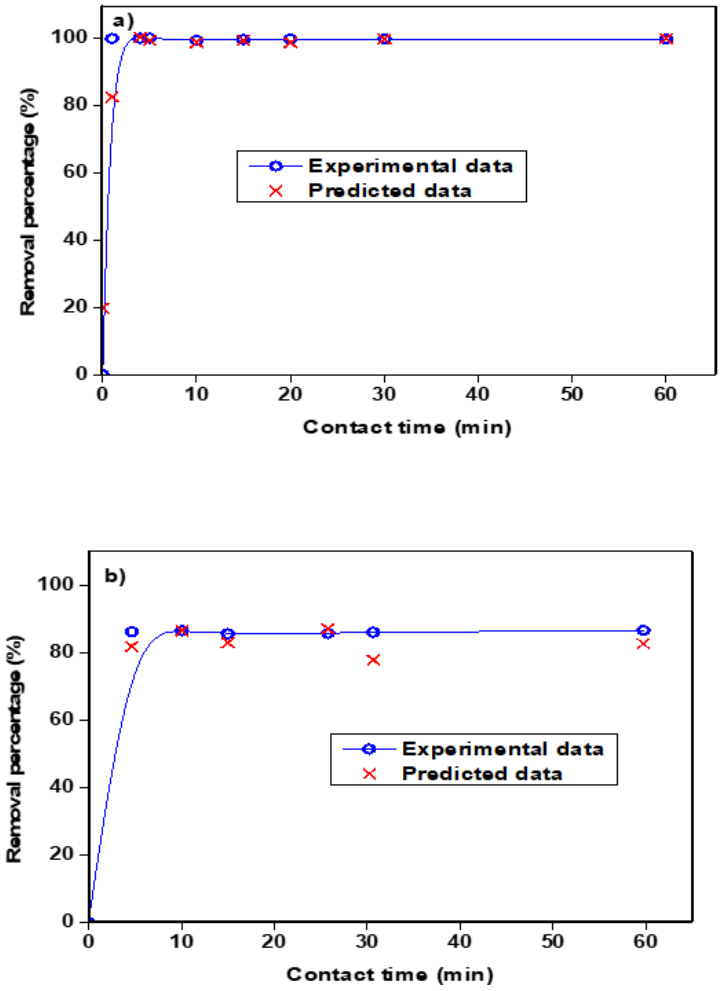


**Figure 6.** Effect of contact time on MG removal (MG concentration: 100 mg/L, adsorbent dose: 1 g/L) of a) commercial bentonite and b) local Algerian bentonite.

### 3.3.2. Effect of adsorbent dose

In order to determine the minimum amount of adsorbent required that is economically feasible in the wastewater treatment process, we studied the effect of the dose of each sorbent on GM removal. As shown in the curve of **Figure 7**, the percentage of MG removal increases with increasing concentration of MG until the mass concentration reaches 0.6 and 1.2 g/L for commercial bentonite and local Algerian bentonite, respectively. This behaviour is due to the high availability of adsorption sites for high concentrations of adsorbent. The saturation of the surface sites is reached at the equilibrium state. The results clearly show that the optimal dose is 0.6 g/L for commercial bentonite and 1.2 g/L for local Algerian

DOI: https://doi.org/10.17509/ijost.v11i1.87371
p- ISSN 2528-1410 e- ISSN 2527-8045

bentonite, which will therefore be selected for subsequent experiments. The data predicted by the ANN are in close agreement with the trends observed experimentally.

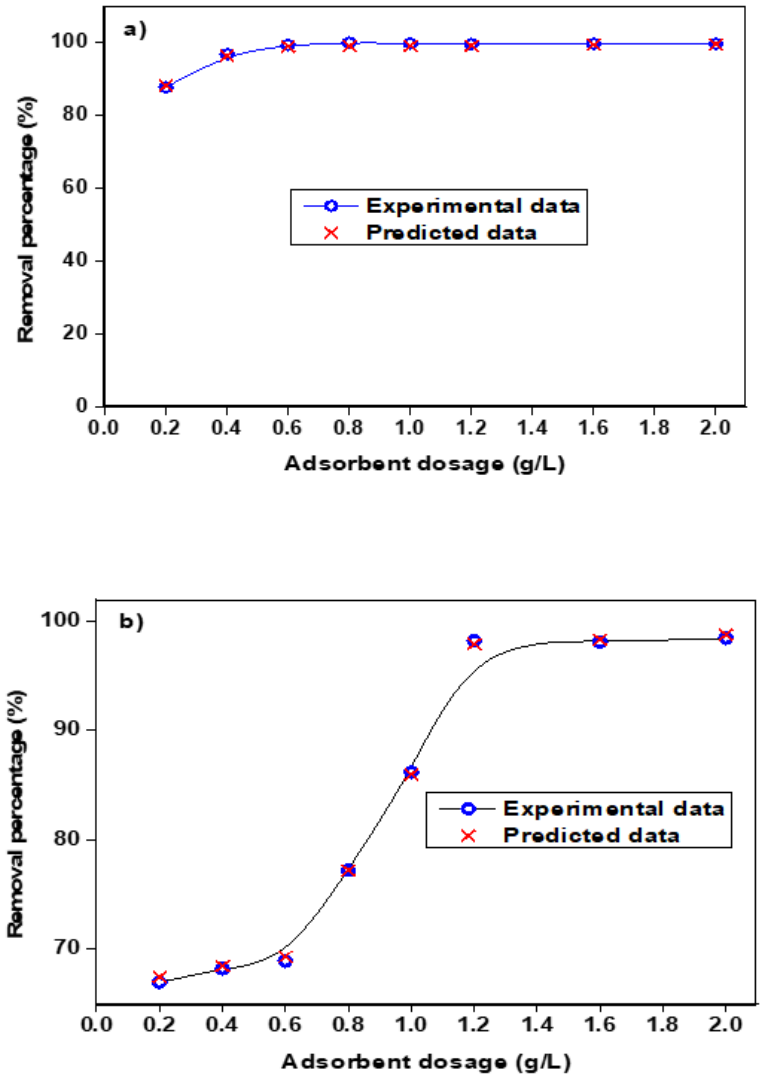


**Figure 7.** Effect of adsorbent dose on MG removal (contact time: 5 min, MG concentration = 100 mg/L) of a) commercial bentonite and b) local Algerian bentonite.

### 3.3.3. Effect of solution pH

The pH variation of the aqueous solution plays an important role in the adsorption process [27]. In this study, the effects of pH on aqueous suspensions are examined in the pH range 2-10 (**Figure 8**). The corresponding results show that the adsorption of MG by local Algerian and commercial bentonite clays was not affected by pH. Similar results have been reported from previous work [28-30]. Based on these results, we retained the pH solution without adjustment for MG in successive experiments.

DOI: https://doi.org/10.17509/ijost.v11i1.87371
p- ISSN 2528-1410 e- ISSN 2527-8045

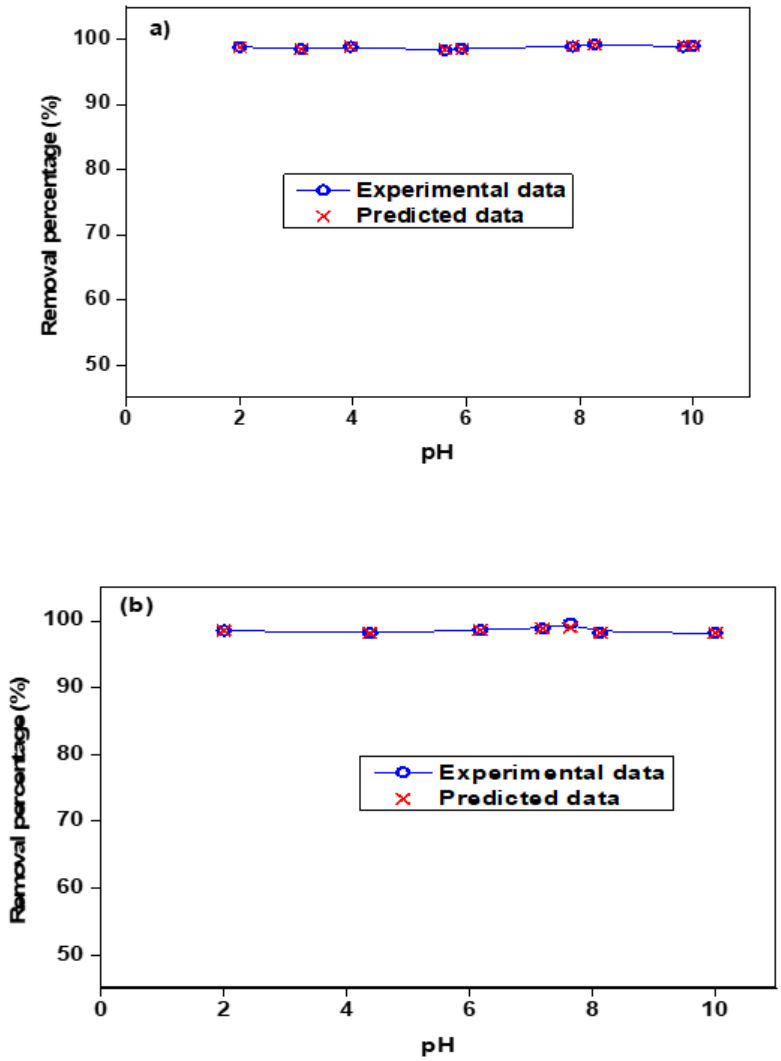


**Figure 8.** Effect of solution pH on MG removal (MG concentration: 100 mg/L, contact time: 5 min, adsorbent dose: 0.6 g/L for commercial bentonite and 1.2 g/L for local Algerian bentonite) of a) commercial bentonite and b) local Algerian bentonite.

### 3.3.4. Effect of MG initial concentration

The initial concentration of MG has a remarkable effect on the MG adsorption in aqueous solutions. Corresponding results shown in **Figure 9** clearly show that the removal percentage of MG decreases slightly with increasing initial concentration. This is explained by the fact that at lower initial concentrations, the report of active surface sites on the adsorbent surface and the dye in solution is high, and therefore, all the MG molecules can be retained by the adsorbents. However, increasing the initial dye concentration slightly reduced the removal efficiency, which can be attributed to the lack of active sites on the adsorbents required for adsorption of high dye concentrations. Similar results have been obtained by previous reports [31,32]. In such conditions, there was a strong correlation between the predicted and experimental data.

DOI: https://doi.org/10.17509/ijost.v11i1.87371
p- ISSN 2528-1410 e- ISSN 2527-8045

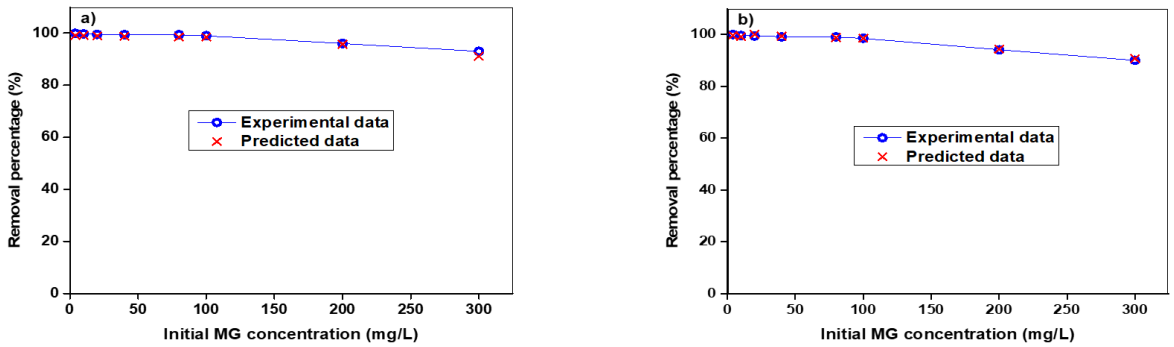


**Figure 9.** Effect of initial MG concentration on MG removal (contact time: 5 min, adsorbent dose: 0.6 g/L for commercial bentonite and 1.2 g/L for local Algerian bentonite, pH: 7) of a) Commercial bentonite and b) local Algerian bentonite.

### 3.3.5. Effect of temperature

Temperature is an important parameter for the adsorption process. To study the influence of temperature on MG dye adsorption by commercial bentonite and local Algerian bentonite, experiments were carried out in the temperature range from 20 to 50°C. Corresponding results in **Figure 10** show that the % removal of MG was decreased from 99.77 to 96.77% and from 98.29 to 95.25% for commercial and local Algerian bentonite clays, respectively, as temperature increased from 20 to 50°C, indicating an exothermic interaction process. The predicted data exhibited good concordance with the experimental measurements. A similar effect has been observed with previously reported [33].

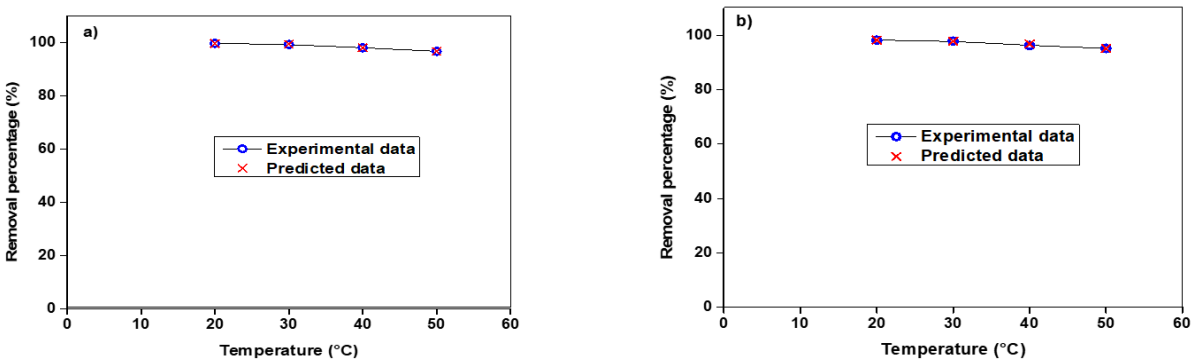


**Figure 10.** Effects of temperature on MG removal (contact time: 5 min, adsorbent dose: 0.6 g/L for commercial bentonite and 1.2 g/L for local Algerian bentonite, pH: 7, MG concentration = 100 mg/L) of a) commercial bentonite and b) local Algerian bentonite.

**Table 6** presents a summary of the results of the training performance, validation performance, and the correlation coefficient in the MG adsorption onto commercial bentonite and local Algerian clays.

The R values are greater than 0.70, indicating that the prediction and experimental data were in agreement and the proposed ANN model exhibited high predictive accuracy for MG adsorption onto the two adsorbents. The lowest values of training and validation performances illustrate the good results given by the ANN model.

DOI: https://doi.org/10.17509/ijost.v11i1.87371
p- ISSN 2528-1410 e- ISSN 2527-8045

**Table 6.** Training, validation performances, and the correlation coefficient in the MG adsorption onto adsorbents.

| Parameter effect | Adsorbent | Training performance | Validation performance | Correlation coefficient (R) |
|---|---|---|---|---|
| Contact time | Commercial bentonite | 0.0383 | 0.0509 | 0.71 |
| | Local Algerian bentonite | $1.9396\times10^{-5}$ | 0.0058 | 0.9963 |
| Adsorbent dosage | Commercial bentonite | 0.0018 | 0.0049 | 0.9874 |
| | Local Algerian bentonite | $3.6575\times10^{-4}$ | 0.0101 | 0.9911 |
| Solution pH | Commercial bentonite | 0.0044 | 0.0237 | 0.9333 |
| | Local Algerian bentonite | $3.5890\times10^{-22}$ | 0.0497 | 0.9280 |
| Initial MG concentration | Commercial bentonite | $1.4001\times10^{-4}$ | 0.0206 | 0.9773 |
| | Local Algerian bentonite | $6.3797\times10^{-4}$ | 0.0068 | 0.9892 |
| Temperature | Commercial bentonite | 0.0020 | $4.2421\times10^{-4}$ | 0.9963 |
| | Local Algerian bentonite | $4.3630\times10^{-15}$ | 0.0184 | 0.9904 |

### 3.3.6. Adsorption isotherms

Experimental results were modeled to understand the interactions between MG and the adsorbent. The models used are Langmuir, Freundlich, and Temkin & Pyzhev (1940) [34-36]. The corresponding linear forms can be expressed using Eqs. (3-5), respectively.

$$C_e/q_e = 1/k_L q_m + C_e/q_m \quad (3)$$

$$\log q_e = \log K_F + 1/n \ (\log C_e) \quad (4)$$

$$q_e = B_T \ln K_T + B_T \ln C_e \quad (5)$$

Where, $q_m$ (mg/g) is the maximum adsorption capacity, $K_L$ (L/mg) is the Langmuir constant, $K_F$ (mg/g) and $n$ are the Freundlich constants, $K_T$ (L/mg) is the Temkin constant, $B_T$ is the constant ($B_T = R.T/b$), $T$ is the temperature (K), $R$ is the universal gas constant (8.314 J/mol.K) and $b$ is the Temkin constant related to heat of adsorption (J/mol).

**Figure 11** presents the adsorption isotherm fitting plots of local Algerian and commercial bentonite clays. **Table 7** summarizes the estimated values of the corresponding parameters.

The coefficient of determination ($R^2$) values in the Freundlich isotherm model are higher than the $R^2$ in the Langmuir and Temkin isotherms, indicating a better fit by this model. Generally, the value of n in the range of 2–10 indicates good, 1–2 moderately difficult, and below 1 poor adsorption characteristics [37]. The measured n was 2 and 2.36 for local Algerian bentonite and commercial bentonite, respectively, which means that the adsorption is favorable.

**Table 7.** Isotherm model parameters for adsorption of MG onto commercial Bentonite and local Algerian bentonite.

| Adsorbent | Langmuir | | | Freundlich | | | Temkin | | |
|---|---|---|---|---|---|---|---|---|---|
| | $R^2$ | $K_L$ (L/mg) | $q_m$ (mg/g) | $R^2$ | $K_F$ (mg/g) | $n$ | $R^2$ | $K_T$ (L/mg) | $B_T$ |
| Commercial bentonite | 0.49 | 0.36 | 400 | 0.90 | 100.69 | 2.36 | 0.16 | 1.00 | 21.22 |
| Local Algerian bentonite | 0.87 | 5.38 | 23.25 | 0.97 | 51.40 | 2 | 0.81 | 39.55 | 25.03 |

DOI: https://doi.org/10.17509/ijost.v11i1.87371
p- ISSN 2528-1410 e- ISSN 2527-8045

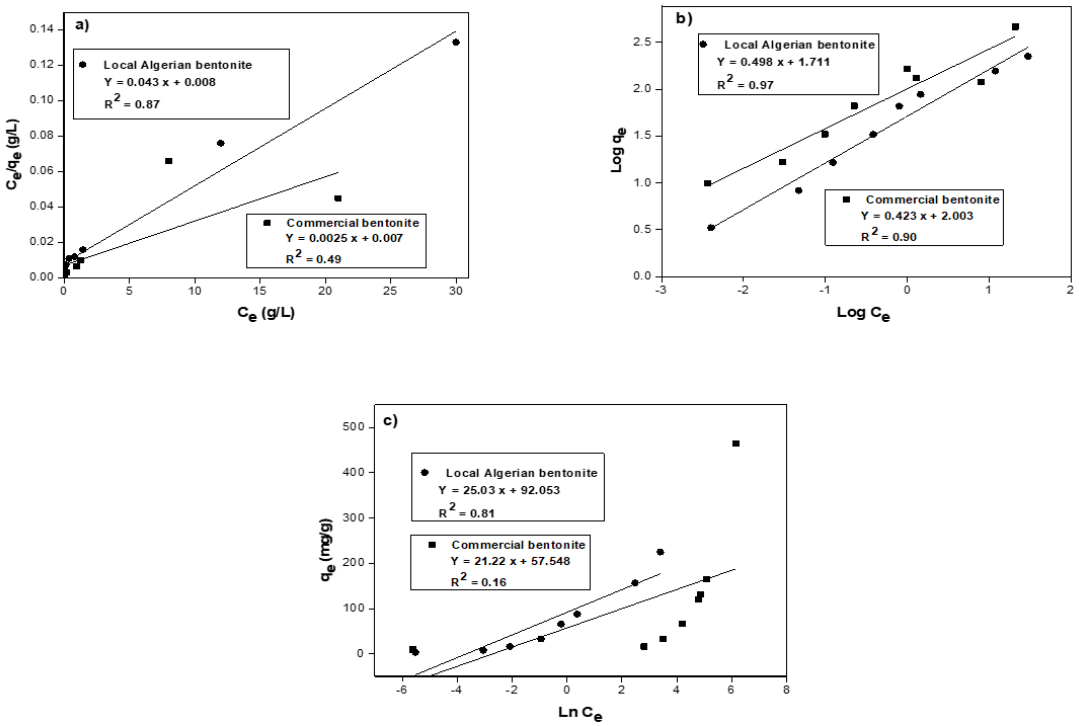


**Figure 11.** Linear a) Langmuir; b) Freundlich, and c) Temkin plots for MG adsorption by commercial bentonite and local Algerian bentonite.

### 3.3.7. Thermodynamic modelling

The adsorption process is often accompanied by thermal effects; thus, the study of thermodynamic parameters is important. Thermodynamic parameters, which include the change in Gibbs' free energy (ΔG˚), enthalpy (ΔH˚), and entropy (ΔS˚), were used to define the thermodynamic behavior of the adsorption of MG onto the adsorbents and were calculated using the following Eq. (6-8) [38].

$$\mathrm{K_c} = q_e \mathrm{m}/C_e \quad (6)$$

$$\mathrm{LnK_c} = \Delta S^{\circ}/R - \Delta H^{\circ}/RT \quad (7)$$

$$\Delta \mathrm{G}^{\circ} = \Delta \mathrm{H}^{\circ} - \mathrm{T}\Delta \mathrm{S}^{\circ} \quad (8)$$

Where, $K_c$ is the thermodynamic equilibrium constant, $q_e$ is the amount of dye adsorbed at equilibrium (mg/g), $m$ is the adsorbent dose (g/L), $C_e$ the equilibrium concentration (mg/L) of the dye in solution, $R$ is the universal gas constant (8.314 J/mol. K) and $T$ is the absolute temperature (K). The values of ΔH° and ΔS° were calculated from the slope and intercept of the van't Hoff scheme of $LnK_c$ against $1/T$ (see Eq. (10)) **(Figure 12)**, and the thermodynamic parameters were summarized in **Table 8**.

The thermodynamic parameters were summarized in **Table 7**. For the two adsorbents, the ΔG° values, which are negative, indicate that the adsorption process is spontaneous and thermodynamically favorable under the experimental conditions. The negative value of ΔH° suggests that the adsorption of MG onto adsorbents is exothermic. In addition, ΔH° values below 80 kJ/mol indicate the process to be physical adsorption. The negative ΔS° value suggests a decline in the disorder at the solid/solution interface during the adsorption. The same results were reported previously in the literature [39].

DOI: https://doi.org/10.17509/ijost.v11i1.87371
p- ISSN 2528-1410 e- ISSN 2527-8045

**Table 8.** Thermodynamic parameters of MG adsorption onto commercial bentonite and local Algerian bentonite.

| Adsorbent | ΔH° (kJ/mol) | ΔS° (J/mol.K) | ΔG° (kJ/mol) | | | |
|---|---|---|---|---|---|---|
| | | | 293 K | 303 K | 313 K | 323 K |
| Local Algerian bentonite | - 22.08 | - 43.42 | - 9.35 | - 8.92 | - 8.48 | - 8.05 |
| Commercial bentonite | - 52.71 | - 126.20 | - 15.73 | - 14.47 | - 13.20 | - 11.94 |

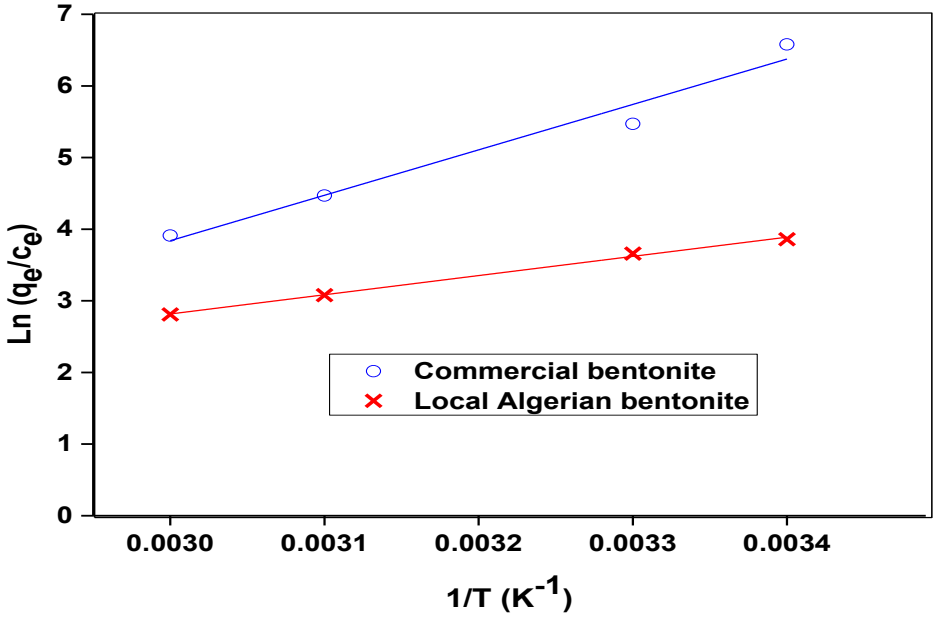


**Figure 12.** Thermodynamic analysis for MG adsorption at different temperatures.

### 3.4. MG Adsorption on Used Clays

The results of this study directly support the essential objectives of sustainable development (SDG) of the United Nations. In this context, the effective removal of the MG dye from aqueous solutions contributes directly to the achievement of SDG 6 (Clean Water and Sanitation) by improving water quality, reducing environmental contamination, and thus protecting human health.

So, it clearly appears that the use of natural and/or modified bentonites that are abundant, economical, and non-toxic in the elimination of organic pollutants in water by adsorption supports SDG 12 (Responsible consumption and production) by promoting the use of sustainable materials in water treatment.

## 4. CONCLUSION

This work investigated the adsorption process of both adsorbents towards MG and developed an ANN model to predict MG adsorption. The used adsorbents were characterized by FTIR, XRF, XRD, and nitrogen adsorption at 77K. The Freundlich model fitted the two equilibrium isotherms. The negative values of ΔG° and ΔH° indicate that the adsorption process was physical, spontaneous, and exothermic. The proposed ANN model 4-10-1 can correlate the adsorption results with acceptable R and MSE. The used clays are therefore

DOI: https://doi.org/10.17509/ijost.v11i1.87371
p- ISSN 2528-1410 e- ISSN 2527-8045

environmentally friendly adsorbents and contribute positively to the objectives of sustainable development of the United Nations.

## 5. ACKNOWLEDGMENT

The authors are thankful to the Faculty of Engineering at Sohar University, Sohar, Oman, for their guidance, technical support, and facilities provided throughout the study.

## 6. AUTHORS' NOTE

The authors declare that there is no conflict of interest regarding the publication of this article. The authors confirmed that the paper was free of plagiarism.

## 7. REFERENCES

[1] Robinson, T., McMullan, G., Marchant, R. and Nigam, P. (2001). Remediation of dyes in textile effluent: a critical review on current treatment technologies with a proposed alternative. *Bioresource Technology*, *77*(3), 247-255.

[2] Rasalingam, S., Peng, P. and Koodali, R. T. (2015). An insight into the adsorption and photocatalytic degradation of rhodamine B in periodic mesoporous materials. *Applied Catalysis B: Environmental*, *174*, 49-59.

[3] Gao, Y., Guo, Y. and Zhang, H. (2016). Iron modified bentonite: Enhanced adsorption performance for organic pollutant and its regeneration by heterogeneous visible light photo-Fenton process at circumneutral pH. *Journal of Hazardous Materials*, *302*, 105-113.

[4] Youssef, E. E., Beshay, B. Y., Tonbol, K. and Sarah O. Makled, S. O. (2023). Biological activities and biosorption potential of red algae (Corallina officinalis) to remove toxic malachite green dye. *Scientific Reports*, *13*(1), 13836.

[5] Rezala, H., Romero, A. and Tidjani, N. (2025). Investigating the comparative adsorption of methyl orange and methyl green on commercial bentonite. *Bulletin of the Chemical Society of Ethiopia*, *39*(4), 643-657.

[6] Alardhi, S. M., Fiyadh, S. S, Salman, A. D. and Adelikhah, M. (2023). Prediction of methyl orange dye (MO) adsorption using activated carbon with an artificial neural network optimization modeling. *Heliyon*, *9*(1), e12888.

[7] Alardhi, S. M., Albayati, T. M., and Alrubaye, J. M. (2020). Adsorption of the methyl green dye pollutant from aqueous solution using mesoporous materials MCM-41 in a fixed-bed column. *Heliyon*, *6*(1), e03253.

[8] Lei, Y., Liu, X., Zhang, J., Dai, Z., Zhao, X. and Liu, G. (2023). A novel composite (ZIF-8@PEI-CC) with enhanced adsorption capacity and kinetics of methyl orange. *Journal of Solid State Chemistry*, *318*, 123758.

[9] Farghali, A. A., Bahgat, M., El Rouby, W. M. A. and Khedr, M. H. (2013). Preparation, decoration and characterization of graphene sheets for methyl green adsorption. *Journal of Alloys and Compounds*, *555*, 193-200.

[10] Perrotti, T.C., Freitas, N.S., Alzamora, M., Sánchez, D.R. and Carvalho, N.M.F. (2019). Green iron nanoparticles supported on amino-functionalized silica for removal of the dye methyl orange. *Journal of Environmental Chemical Engineering*, *7*(4), 103237.

[11] Naeem, A., Saeed, T., Sayed, M., Ahmad, B., Mahmood, T., Farooq, M. and Perveen, F. (2023). Chitosan decorated zirconium metal-organic framework for collaborative adsorption and photocatalytic degradation of methylene blue and methyl orange. *Process Safety and Environmental Protection*, *176*, 115-130.

[12] Ewis, D., Ba-Abbad, M. M., Benamor, A. and El-Naas, M. H. (2022). Adsorption of organic water pollutants by clays and clay minerals composites: A comprehensive review. *Applied Clay Science*, *229*, 106686.

[13] Isah B. A., Ponnuchamy, M., Senthil Rathi, B., Senthil Kumar, P., Kapoor, A., Rajagopal, M., Awasthi, A. and Rangasamy, G. (2024). Artificial intelligence-based neural network modeling of adsorptive removal of phenol from aquatic environment. *Desalination and Water Treatment*, *319*, 100564.

[14] Al-Musawi, T. J., Arghavan, S. M. A, Allahyari, E., Arghavan, F. S, Othmani, A and Nasseh, N. (2023). Adsorption of malachite green dye onto almond peel waste: a study focusing on application of the ANN approach for optimization of the effect of environmental parameters. *Biomass Conversion and Biorefinery*, *13*, 12073–12084.

[15] Wang, X., Liu, S., Chen, S., He, X., Duan, W., Wang, S., Zhao, J., Zhang, L., Chen, Q. and Xiong, C. (2024). Prediction of adsorption performance of ZIF-67 for malachite green based on artificial neural network using L-BFGS algorithm. *Journal of Hazardous Materials*, *473*, 134629.

[16] Parsazadeh, N., Yousefi, F., Ghaedi, M., Dashtian, K. and Borousan, F. (2018). Preparation and characterization of monoliths HKUST-1 MOF via straightway conversion of Cu(OH)2-based monoliths and its application for wastewater treatment: Artificial neural network and central composite design modeling. *New Journal of Chemistry*, *42*(12), 10327-10336.

[17] Khalaf, H., Bouras O. and Perrichon V. (1997). Synthesis and characterization of Al-pillared and cationic surfactant modified Al-pillared Algerian bentonite. *Microporous Materials*, *8*(3-4), 141-150.

[18] Qlihaa, A., Dhimni, S., Melrhaka, F., Hajjaji, N. and Srhiri, A. (2016). Physico-chemical characterization of a Morrocan clay. *Journal of Materials and Environmental Science*, *7*, 1741-1750.

[19] Al-Zubaidi, N. S., Alwasiti, A. A. and Mahmood, D.A. (2017). Comparison of nano bentonite and some nano chemical additives to improve drilling fluid using local clay and commercial bentonites. *Egyptian Journal of Petroleum*, *26*(3), 811-818.

[20] Kumar, A. and Lingfa, P. (2020). Sodium bentonite and kaolin clays: Comparative study on their FTIR, XRF, and XRD. *Materials Today: Proceedings*, *22*(3), 737-742.

[21] Wang, H. L., Gao Q. M. and Hu, J. (2009). High hydrogen storage capacity of porous carbons prepared by using activated carbon. *Journal of the American Chemical Society*, *131*(20), 7016-7022.

[22] Rezala, H., Douba, H., Boukhatem, H. and Romero, A. (2020). Adsorption of methylene blue by hydroxyl-aluminum pillared montmorillonite. *Journal of The Chemical Society of Pakistan*, *42*(4), 550-563.

[23] Rezala, H., Romero, A. and Tidjani, N. (2025). Investigating the comparative adsorption of methyl orange and methyl green on commercial bentonite. *Bulletin of the Chemical Society of Ethiopia*, *39*(4), 643-657.

[24] Brunauer, S., Deming, L. S., Deming W. E. and Teller, E. (1940). On a Theory of the van der Waals Adsorption of Gases. *Journal of the American Chemical Society*, *62*(7), 1723-1732.

[25] Sing, K. S. W., Everett, D. H., Haul, R. A. W., Moscou, L., Pierotti, R. A., Rouquerol J. and Siemieniewska, T. (1985). Reporting physisorption data for gas/solid systems with special reference to the determination of surface area and porosity. *Pure and Applied Chemistry*, *57*(4), 603-619.

DOI: https://doi.org/10.17509/ijost.v11i1.87371
p- ISSN 2528-1410 e- ISSN 2527-8045

[26] Bukka, K., Miller, J. D. and Shabtai, J. (1992). FTIR study of deuterated montmorillonite: Structural features relevant to pillared clay stability. *Clays and Clay Minerals*, *40*(1), 92-102.

[27] Elmoubarki, R., Mahjoubi, F. Z., Tounsadi, H., Moustadraf, J., Abdennouri, M., Zouhri, A., ElAlban A. and Barka, N. (2015). Adsorption of textile dyes on raw and decanted Moroccan clays: kinetics, equilibrium and thermodynamics. *Water Resources and Industry*, *9*, 16-29.

[28] Santos, S. C. R., Oliveira A. F. M and Boaventura, R. A. R. (2016). Bentonitic clay as adsorbent for the decolourisation of dye house effluents. *Journal of Cleaner Production*, *126*, 667-676.

[29] Al-Futaisi, A., Jamrah, A. and Ai-Hanai, R. (2007). Aspects of cationic dye molecule adsorption to palygorskite. *Desalination*, *214*(1-3), 327-342.

[30] Roulia, M.A. and Vassiliadis, A. (2008). Sorption characterization of a cationic dye retained by clays and perlite. *Microporous and Mesoporous Materials*, *116*(1-3), 732-740.

[31] Meskel, A. G., Kwikima, M. M., Meshesha, B. T., Habtu, N. G., Chinna Swami Naik, S. V. and Vellanki, B. P. (2024). Malachite green and methylene blue dye removal using modified bagasse fly ash: Adsorption optimization studies. *Environmental Challenges*, *14*(5), 100829.

[32] Somsiripan, T. and Sangwichien, C. (2023). Enhancement of adsorption capacity of Methylene blue, Malachite green, and Rhodamine B onto KOH activated carbon derived from oil palm empty fruit bunches. *Arabian Journal of Chemistry*, *16*(12), 105270.

[33] Jabar, J. M., Adebayo, M. A., Odusote, Y. A., Yılmaz, M. and Rangabhashiyam, S. (2023). Valorization of microwave-assisted H3PO4 activated plantain (*Musa paradisiacal L*) leaf biochar for malachite green sequestration: models and mechanism of adsorption. *Results in Engineering*, *18*(5), 101129.

[34] Langmuir, I. (1916). The constitution and fundamental properties of solids and liquids. *Journal of the American Chemical Society*, *38*, 2221-2295.

[35] Freundlich, H. M. F. (1906). Uber die adsorption in Losungen. *Zeitschrift fur Physikalische Chemie*, *57*, 385–470.

[36] Temkin, M. J. and Pyzhev, V. (1940). Recent modifications to Langmuir isotherms. *Acta Physicochimica U.R.S.S*, 12, 217-225.

[37] Amin, M.T., Alazba A.A. and Shafiq, M. (2015). Adsorptive removal of reactive black 5 from wastewater using bentonite clay: Isotherms, kinetics and thermodynamics. *Sustainability*, *7*(11), 15302-15318.

[38] Boukhatem, H., Ouazene, N., Rezala, H., Djouadi, L., Selami, S. and Zeraif, S. (2023). Removal of methylene blue dye from aqueous media by adsorption using nickel oxide modified montmorillonite composite. *Indian Journal of Chemical Technology*, *30*(6), 812-821.

[39] Bessaha, F., Marouf-Khelifa, K., Batonneau-Gener, I. and Khelifa, A. (2016). Characterization and application of heat-treated and acid-leached halloysites in the removal of malachite green: adsorption, desorption, and regeneration studies. *Desalination and Water Treatment*, *57*(31), 14609–14621.

DOI: https://doi.org/10.17509/ijost.v11i1.87371
p- ISSN 2528-1410 e- ISSN 2527-8045